Novel hybrid based on a poly[Ni(*salen*)] film and WO_3 nanoparticles with electrochromic properties

Marta Nunes[a], Cosme Moura[b], A. Robert Hillman[c] and Cristina Freire[a*]

[a] REQUIMTE/LAQV, Departamento de Química e Bioquímica, Faculdade de Ciências, Universidade do Porto, 4169-007 Porto, Portugal.

[b] CIQ, Departamento de Química e Bioquímica, Faculdade de Ciências, Universidade do Porto, 4169-007 Porto, Portugal.

[c] Department of Chemistry, University of Leicester, Leicester LE1 7 RH, UK.

*Corresponding author: Professor Dr. Cristina Freire (acfreire@fc.up.pt), Dr. Marta Nunes (marta.nunes@fc.up.pt)

Tel.: +351 22 04020590; Fax: +351 22 0402 695

ABSTRACT

The strategy of combining electroactive polymers and inorganic nanomaterials has been widely explored in recent years in order to improve some of their properties, namely electrocatalysis and electrochromism. This report focuses on a new composite prepared through the electropolymerization of the transition metal complex [Ni(3-Mesalen)], designated as [1], in the presence of WO_3 nanoparticles (NPs) and its electrochromic (EC) performance. The WO_3 NPs were prepared using tungsten metal powder; their characterization indicated quasi-spherical morphology, high crystallinity and particle sizes in the range 30 – 40 nm. The nanocomposite WO_3@poly[1] films displayed similar electrochemical responses to those of pristine poly[1] films in $LiClO_4/CH_3CN$, but higher electroactive surface coverages, an advantage of NPs incorporation in the nanocomposite. The presence of the WO_3 NPs in the poly[1] matrix was assessed by X-ray photoelectron spectroscopy and scanning electronic microscopy. The nanocomposite presented similar electronic spectra to those of poly[1], indicating that the electronic structure of the pristine film is maintained in the nanocomposite, but exhibited lower ε-values for bands associated with charge transfer transitions for high oxidised states, revealing an enhanced stability towards ligand over-oxidation.

The WO_3@poly[1] nanocomposite showed more favourable EC properties in $LiClO_4/CH_3CN$ than the pristine film. For typical coverages (Γ = 0.06-0.10 μmol cm^{-2}) the composite showed lower switching times (τ = 1.3 - 3.6 s), higher optical contrast (ΔT ≈ 31 %, an improvement of ca. 40 %) and better colouration efficiencies (in the range η = 104 - 115 cm^2 C^{-1}, improvement of ca. 13 - 22 %).

Keywords: Electrochromism; Electroactive polymers; Metal *salen* complexes; Tungsten trioxide; Polymeric nanocomposites.

1. INTRODUCTION

The science and technology of conducting polymers (CPs, also called conjugated polymers or synthetic metals) have travelled a long way since the discovery of polyacetylene in 1970 [1,2]. These materials are characterized by a backbone based on alternating single/double bonds, typically formed from aromatic monomers (e.g. thiophenes, pyrroles and anilines), and have the ability to undergo reversible oxidation (p-doping) and reduction (undoping), which allow them to switch between neutral (insulating) and oxidised (conducting) forms [3].

In recent years, there has a noticeable shift in emphasis towards the application of CPs in practical devices. Quite generally, this requires physicochemical attributes that are not possessed by a single material: hybrid materials provide one approach to exploiting this, particularly if they combine organic and inorganic materials at an intimate level using nanoscale material. The value of this approach is exemplified by organic/inorganic hybrid assemblies based on the combination of CPs with, for example, metal nanoparticles [4], carbon nanostructures [5,6] and inorganic compounds [7]. Combination of CPs with metal oxide semiconductors constitute, undoubtedly, one of the most promising classes [8,9], since they combine the elasticity and functionality of the CPs with the high thermal and chemical stabilities of metal oxides [10]. Reported examples of such composites include the incorporation of TiO_2 [11-13], ZnO [14] and MnO_2 [15] nanomaterials in CP matrices. In particular, tungsten(VI) oxide (WO_3), an n-type semiconductor with a band gap of 2.7 eV [8], has been widely employed to assemble WO_3/CPs nanocomposites for applications as sensors [16-18] and electrocatalysts [19], mainly due to its ability to intercalate electrons and protons [20].

WO_3 is the mostly investigated inorganic electrochromic material [21,22] due to its good chemical stability, strong adherence to substrate and genuine colour switching

(cathodic EC material) [23,24]. These properties make it an attractive "partner" for CPs (or other electroactive polymers) in hybrid materials for EC applications. In fact, several EC nanocomposites based in the incorporation of WO_3 nanostructures into CP matrices, such as polyaniline (PANI) [23-27] and poly(3,4-ethylenedioxythiophene) (PEDOT) [28], have already been reported, exploiting the complementary EC attributes of WO_3 and CPs. In general, CPs exhibit interesting optical properties, with rich colour changes due to their multiple redox states, but have low colour switching rates due to the slow transport of charge balancing counter ions ("dopants") into the polymer layer. On the other hand, metal oxide nanostructures have high surface-to-volume ratio and organized structures that facilitate ion/electron intercalation processes and promote switching reversibility [10,29]. Thus, the resultant nanocomposites promise the advantage of synergistic influence of the WO_3 on the EC properties of conducting polymer, presenting improved EC properties with more satisfactory switching speeds and colouration efficiencies [23,25,27].

The poly[M(*salen*)]-type films (M ≡ transition metal) are a particular class of electroactive metallopolymers, derived from metal *salen* complexes, recently studied by their interesting EC behavior [30,31]. These electroactive polymers combine the robustness of the *salen* ligand with its ability to coordinate several transition metal centers, which is a powerful tool to prevent structural defects and thus facilitate the mobility of charge carriers [32,33]. The similarity of poly[M(*salen*)]-based films with CPs, namely in the poly(phenylene)-based redox properties and their rich coloured redox states, makes them interesting EC polymers.

This work reports the preparation and characterization of a novel composite film based in the incorporation of WO_3 NPs into the matrix of a poly[Ni(*salen*)]-based film and the evaluation of its EC properties. The metal *salen* polymer employed was

poly[Ni(3-Mesalen)], designated by poly[1]. The EC performance evaluation of the pristine poly[1] was already reported [34] and showed promising EC properties, with a good electrochemical stability - a charge loss of 34.3 % after ≈ 9000 cycles - and interesting colour changes, from yellow in the neutral state to green and russet (reddish-brown) in the oxidised states. Nonetheless, in order to realize commercial application, the EC properties of poly[1] need to be improved, particularly in terms of response time and colouration efficiency. Thus, we took the advantages of WO_3 NPs properties - nanometric size (high surface-to-volume ratio) and semiconductor properties - to incorporate them within poly[1] and to evaluate their influence on the composition, morphology, electrochemical response and spectroelectrochemical properties, with the ultimate goal to achieve enhanced EC properties. The hybrid films were prepared through the *in situ* electropolymerization of the Ni-*salen* complex in the presence of the WO_3 NPs; this method has several advantages, notably formation and surface immobilization of the metallo-organic/inorganic composite in a single step [29,35]. To the best of our knowledge, this is the first time that metallopolymer-nanoparticle hybrid films between this family of M-*salen* polymers and WO_3 NPs have been prepared.

2. EXPERIMENTAL SECTION

2.1 Materials and instrumentation

Tungsten metal powder (Alfa Aesar, 99.9 %), hydrogen peroxide (Aldrich, 30 wt.% in H_2O), glacial acetic acid (Merck, 100 %), acetonitrile and propylene carbonate (PC) (Romil, pro analysis grade) and $LiClO_4$ (Aldrich, 99 %) were used as received; ultra-pure water (resistivity 18.2 MΩ cm at 25 ºC, Millipore) was used. The complex *N,N'*-bis(3-methylsalicylideneiminate) nickel(II), [Ni(3-Mesalen)], and respective *salen* ligand were prepared by methods described in the literature [36]. Briefly, the *salen* ligand H_2(3-

Mesalen) was synthesized by refluxing (for 5 hours) a methanol solution containing ethylenediamine and 2-hydroxy-3-methylbenzaldehyde (molar ratio = 2:1); on cooling to room temperature, the yellow solid formed was filtered off and dried under vacuum. The complex [Ni(3-Mesalen)] was prepared by refluxing (for 5 hours) a methanol solution containing stoichiometric amounts of nickel (II) acetate and the ligand H_2(3-Mesalen); after cooling, a red-brown solid was filtered off and dried under vacuum.

Powder X-ray diffraction (XRD) measurements were performed at Departamento de Química, CQ-VR, Universidade de Trás-os-Montes e Alto Douro (Vila Real, Portugal), at room temperature using a PW 3040/60 X'Pert Pro Röntgen diffractometer with Cu Kα radiation (λ = 1.5418 Å) and $\theta/2\theta$ Bragg-Brentano configuration, over the 2θ range of 15–80º. The system includes the ultrafast PW3015/20 X'Celerator detector and a secondary monochromator. The diffractograms were treated with the Le Bail method [37,38].

X-ray photoelectron spectroscopy (XPS) analyses were performed at Centro de Materiais da Universidade do Porto (CEMUP), Porto, Portugal, in a Kratos AXIS Ultra HAS spectrometer, using a monochromatic Al Kα radiation (1486.7 eV). The XPS spectra were deconvoluted with the XPSPEAK 4.1 software, using a non-linear least squares fitting routine after a Shirley-type background subtraction. To correct possible deviations caused by sample charging, the C1s peak at 284.6 eV was used as an internal reference. The surface atomic percentages were calculated from the corresponding peak areas, using sensitivity factors provided by the manufacturer.

Fourier transform infrared (FTIR) spectra were obtained on a Jasco FT/IR Plus Spectrophotometer in the 4000 – 400 cm^{-1} region, with a resolution of 4 cm^{-1} and averaged over 32 scans. The sample materials were diluted with KBr (99 %, spectroscopic grade, Sigma-Aldrich) and studied as pellets containing 1.4 wt. % of sample.

Transmission electron microscopy (TEM) images were collected at HEMS/IBMC – Histology and Electron Microscopy Service – Institute for Molecular and Cell Biology (IBMC) of the Universidade do Porto. The sections were examined under a JEOL JEM 1400 TEM (Tokyo, Japan) equipped with an EDX Microanalysis System (Oxford Instruments, Abingdon, UK); the images were digitally recorded using a Gatan SC 1000 ORIUS CCD camera (Warrendale, PA, USA). To prepare the sample, a small amount of NPs was dispersed in ethanol under sonication. Afterwards, a carbon-coated 400 mesh copper grid was immersed in the resulting solution, followed by air-drying. After the evaluation of the TEM images, the diameter of 100 particles was measured to generate a histogram and calculate the average particle size distribution.

Scanning electron microscopy/energy-dispersive X-Ray spectroscopy (SEM/EDS) analysis was performed at CEMUP, using a High-Resolution (Schottky) Environmental Scanning Electron Microscope with X-Ray Microanalysis and Electron Backscattered Diffraction analysis (Quanta 400 FEG ESEM / EDAX Genesis X4M).

Electrochemical studies were performed using an Autolab PGSTAT 30 potentiostat/galvanostat (EcoChimie B.V.), controlled by GPES software. The studies were performed using a three-electrode cell with a single or separate (for chronoamperometric studies) compartments, enclosed in a grounded Faraday cage. The reference electrode was an Ag/AgCl (1.0 mol dm^{-3} NaCl) electrode (Metrohm ref. 6.0724.140). A Pt wire or a Pt plate (for the separate compartment cell) was used as the counter electrode. The working electrode was indium tin oxide coated poly(ethylene terephthalate) (ITO/PET) (Aldrich, resistivity of 60 Ω sq^{-1}) and a Pt disk (area 0.0314 cm^2, BAS) for coulometric studies. The Pt disk was polished with aluminium oxide of particle size 0.3 μm (Buehler) on a microcloth polishing pad (Buehler), then washed with ultra-pure water and CH_3CN before use.

The spectroelectrochemical studies were performed *in situ* using an Agilent 8453 spectrophotometer (with diode array detection) coupled to the potentiostat/galvanostat. The spectroelectrochemical cell was made from Teflon; it comprised an Ag/AgCl (3.0 mol dm^{-3} NaCl) (Bio-Logic) reference electrode, a Pt grid counter electrode and ITO/PET (typical area 0.785 cm^2) working electrode.

2.2 Preparation of WO_3 NPs

WO_3 NPs were prepared by a procedure adapted from the literature [39,40]. Briefly, 6.5 g of tungsten metal powder were dissolved in 40 mL of 30 wt.% H_2O_2 and 4 mL of millipore water, until a colourless solution was obtained. This solution was filtered and refluxed at 55 ºC for 17 hours, after the addition of 40 mL of glacial acetic acid. A yellow flaky solid was obtained after solvent evaporation, which was heated to 100 ºC (5 ºC / min) in air, held at this temperature for 1 h, and then brought back to room temperature. Finally, separate samples were annealed at three different temperatures (250, 450 or 550 ºC) for 2 hours, at the same heating rate.

2.3 Film preparation and electrochemical characterization

The WO_3@poly[1] films were prepared by cyclic voltammetry (CV) from solutions containing 1.0 mmol dm^{-3} [Ni(3-Mesalen)] (complex [1]) and 5 wt.% (WO_3/$LiClO_4$ wt.%) of WO_3 NPs (annealed at 550 ºC) in 0.1 mol dm^{-3} $LiClO_4/CH_3CN$. Prior to electrodeposition, the starting solutions were (i) sonicated ("s") during 10 minutes or (ii) sonicated during 10 minutes followed by reflux ("r") for 3 hours; procedure (ii) was made to evaluate the influence of the reflux step in the dispersion of the WO_3 NPs and monomer adsorption on WO_3 NPs surface. The potential of the working electrode (ITO/PET 2.25 cm^2) was cycled between 0.0 and 1.3 V at 0.020 V s^{-1}, for 10 scans. According to the

method used, the resulting films are designated WO_3@poly[1]_s and WO_3@poly[1]_r, respectively. Pristine poly[1] films were prepared using the same experimental conditions, but in the absence of WO_3 NPs.

Upon film deposition, the modified electrodes were rinsed with dry CH_3CN or PC, immersed in monomer- and WO_3-free 0.1 mol dm^{-3} $LiClO_4/CH_3CN$ or $LiClO_4$/PC solutions and redox cycled in the potential ranges -0.1 to 1.2 V or -0.1 to 1.3 V, respectively, at 0.010 V s^{-1}, during 5 redox cycles. The electroactive surface coverage of each film, Γ/ μmol cm^{-2} (cited in terms of monomer units) was determined by a coulometric assay in monomer/WO_3 free solution, based on integration of the complete voltammetric (*i*-*E*) anodic response ($Q = nFA\Gamma$); the same doping level value n = 0.65 for the original and nanocomposite films was used, based in the assumption that WO_3 incorporation did not affect the film overall redox processes, as verified in a previous study with Ni-*salen* nanocomposite and multi-walled carbon nanotubes [41], and that WO_3 is not electroactive in the potential range used. The *n* value was calculated from the ratio of the anodic charge passed during 1-cycle electropolymerization film to the anodic charge of the corresponding as-prepared film redox switching (Q_{pol}/Q_{redox}), as described in literature [42]. The voltammograms used in the calculation of Γ values were performed in monomer- and WO_3-free in 0.1 mol dm^{-3} $LiClO_4/CH_3CN$ solution at the scan rate of 0.010 V s^{-1}, to ensure that the oxidation/reduction processes occur throughout the whole film. For the films reported here, the peak current was linear with potential scan rate in this potential scan rate range, so we ensure complete film redox conversion, giving a correct coulometric assay; at substantially higher scan rates, this was not always the case.

2.4 Composition and morphology characterization

The compositional and morphological characterizations of WO_3@poly[1]_r nanocomposite were performed by XPS and SEM/EDS, respectively. All films were analysed after emersion in the reduced state. XPS was also used to investigate the influence of redox cycling on film chemical composition. Films were analysed: (i) immediately after polymerization, i.e. before redox cycling, by application of E = 0.0 V for 200 s in 0.1 mol dm^{-3} $LiClO_4/CH_3CN$ (to ensure establishment of the reduced state); (ii) after potential cycling (-0.1 to 1.2 V) in 0.1 mol dm^{-3} $LiClO_4/CH_3CN$; and (iii) after potential cycling (-0.1 to 1.3 V) in 0.1 mol dm^{-3} $LiClO_4$/PC. In the latter two instances, 5 potential cycles were imposed, at ν = 0.020 V s^{-1}. Poly[1] films were studied under identical conditions for comparison purposes.

2.5 Spectroelectrochemical characterization

Film redox chemistry was studied by *in situ* UV-Vis spectroscopy: the sample films were prepared with 3 electrodeposition cycles, at ν = 0.020 V s^{-1} and redox cycled in 0.1 mol dm^{-3} $LiClO_4/CH_3CN$ and $LiClO_4$/PC supporting electrolytes, as described in section 2.3. The UV-Vis spectra were acquired simultaneously with the *i-E* curves, at intervals of 0.5 s (i.e. 10 mV potential resolution), in the wavelength range 315 – 1100 nm, during the 4^{th} redox cycle (as a representative response). The molar extinction coefficients, ε / cm^{-1} mol^{-1} dm^3, of all observed electronic bands were estimated using a combination of the Beer-Lambert and Faraday laws (Equation 1) [32,33,43]:

$$Abs(\lambda) = \varepsilon(\lambda)\, Q / nFA \qquad (1)$$

where Q is the charge (C), n is the doping level, F is the Faraday constant and A the electrode area (cm^2).

2.6 Electrochromic properties evaluation

The EC parameters – switching times (τ), optical contrast (ΔT%), change of the optical density (ΔOD) and colouration efficiency (η) - of the nanocomposite films were obtained by a double potential step method (chronoamperometry) coupled with UV-Vis spectroscopy (chronoabsorptometry). The studies were performed in 0.1 mol dm^{-3} $LiClO_4/CH_3CN$ and $LiClO_4$/PC solutions, focusing on the first oxidation stage (associated with the colour transition yellow ↔ green), which proved to be the most promising for pristine poly[1] [34]. In the double potential step experiment, the potential was set at the initial potential of E = 0.0 V for 50 s, then stepped to a second potential E = 0.7 V for 50 s, and finally switched back to the initial potential. Simultaneous with the chronoamperometric response, chronoabsorptometric measurements were performed at the fixed wavelength of λ = 750 nm, acquiring the UV-Vis spectra at 1 s intervals during 4 double potential steps. The films studied were electrodeposited during 3 cycles, using the typical experimental conditions. The ΔOD was calculated using Equation 2 [44]:

$$\Delta OD\ (\lambda) = \log\ (T_{red}(\lambda) / T_{ox}(\lambda)) \quad (2)$$

where T_{red} and T_{ox} are the transmittance values of the films in reduced and oxidized states, respectively, at λ = 750 nm. The colouration efficiency (η / $cm^2\ C^{-1}$) was measured by the relation between ΔOD and the amount of injected/ejected charge per unit area, Q_d, necessary to induce the full switch, given by the Equation 3 [44,45]:

$$\eta = \Delta OD / Q_d \quad (3)$$

The optical switching times were defined as the time taken for 90% of the total absorbance change [46,47]. The electrochemical stability was evaluated by a chronoamperometry experiment, using the same experimental conditions, but over an extended cycling interval (ca. 9500 redox cycles, taking ca. 11 days) on films prepared by 10 electrodeposition cycles. For comparison purposes, analogous EC parameters were also evaluated for a pristine poly[1] film subject to the same protocol.

3. RESULTS AND DISCUSSION

3.1 WO_3 NPs characterization

The XRD patterns of the WO_3 NPs annealed at 450 and 550 ºC are shown in Figure 1 (a); analogous data for material annealed at 250 ºC are depicted in Figure S1 in Supporting Information (SI).

Figure 1

The XRD pattern of NPs annealed at 250 ºC exhibits two broad peaks in the $2\theta \approx$ 20 – 39º and 42 – 68 º ranges, indicating an amorphous structure [40]. In contrast, the patterns of NPs annealed at 450 and 550 ºC show well defined peaks typical of crystalline NPs. The NPs annealed at 550 ºC, show the highest intensity and sharpest peaks, reflecting an enhancement of crystallinity with increased annealing temperature. The XRD peaks of both NPs annealed at 450 and 550 ºC (2θ = 23.0, 23.5, 24.2, 26.5 and 28.6 º) are indexed, respectively, to the (002), (020), (200), (120) and (112) planes and are in accordance with a monoclinic WO_3 structure (JCPDS no. 83-0950); no other peaks were observed pertaining to other WO_3 structures. The mean crystallite sizes of the NPs annealed at 450 and 550 ºC are 30.5 and 40.2 (± 1.0) nm, respectively.

The SEM and TEM micrographs obtained for WO_3 NPs annealed at 550 ºC are depicted in Figures 1 (b) and S2 in SI, respectively. Both micrographs show quasi-spherical WO_3 NPs. The particle size distributions were fitted by a log-normal function (Figure S3), leading to an average particle size of 38 nm (± 4 nm) by SEM and 35 nm (± 8 nm) by TEM; the values obtained by the two techniques are similar and are in agreement with those obtained by XRD.

The FTIR spectra of WO_3 NPs annealed at different temperatures are depicted in Figure S4, in SI. In all spectra there is a large band in the range 1000-500 cm^{-1} that is characteristic of the W-O and O-W-O stretching vibrations [48,49]. The spectra of NPs annealed at the highest temperatures (450 and 550 ºC) exhibit one vibration band at 1037 cm^{-1}, which is assigned to the W=O stretching modes [50]. Furthermore, all the spectra also exhibit a very broad band with a maximum at 3098 cm^{-1} and a weak band at 1613 cm^{-1} that correspond to O-H stretching and bending vibrations, respectively [51], due to the presence of adsorbed water and/or hydroxylated W-OH bonds. This broad band is more intense in the spectrum of the WO_3 NPs annealed at 250 ºC and decreases in intensity with increased annealing temperature. The vibration bands at 1705 cm^{-1} and 1537-1403 cm^{-1}, clearly seen in the spectrum of the latter NP, are assigned to the C=O stretching vibrations and C-H bending vibrations [52] from acetic acid used in the synthesis, that may still be adsorbed at the lowest annealing temperature. These vibration bands decreased in intensity in the spectra of NPs annealed at 450 and 550 ºC, which reflects the degradation / elimination of these contaminants at the highest annealing temperatures.

High-resolution XPS spectra in the W4f and O1s regions for the WO_3 NPs annealed at 550 ºC (see Figure S5 in SI) show two main W4f peaks (at 35.6 and 37.8 eV; doublet separation Δ = 2.20 eV and an peak areas ratio 0.75), which are assigned to the $W^{(VI)}$ $4f_{7/2}$ and $W^{(VI)}$ $4f_{5/2}$ levels of W in +6 oxidation state in WO_3, respectively [49,53]. The other two peaks with smaller intensities (at 34.3 and 36.6 eV) are assigned to $W^{(V)}$ $4f_{7/2}$ and $W^{(V)}$ $4f_{5/2}$ levels, respectively [54]; the presence of tungsten in a lower oxidation state, $W^{(V)}$, is probably as a result of X-ray radiation reduction that may occur during XPS data acquisition. In the O1s region three peaks are observed: a main peak at 530.4 eV assigned to the lattice oxygen bonded to W [55], a peak at 531.5 eV due to –OH groups and possible

C=O groups and a peak at 532.6 eV attributed to C-O bonds, probably from acetic acid residues [49,54]. The atom percentages, 19.9 % of W and 80.1 % of O, give a higher O/W atomic ratio ($O/W_{obtained}$ = 4.0) compared the expected value ($O/W_{theoretical}$ =3.0). We attribute this to residual acetic acid surface contamination, during the NPs synthesis.

3.2 Electrochemical preparation and characterization of WO_3@poly[1]

Two type of nanocomposite films were prepared, using solutions containing the [Ni(3-Mesalen)] complex and 5 wt.% of WO_3 NPs, previously either (i) sonicated or (ii) sonicated and refluxed. Based on the materials characterization described above, attention was focused in composites incorporating the WO_3 NPs annealed at 550 ºC, which have more well-developed crystallinity, since a well-organized structure can be advantageous in electrochemical/electrochromic applications [56]. It is worth mention that WO_3 is a cathodic EC material, which is uncolored in the potential range explored in this work and thus its intrinsic redox activity and EC behavior is not discussed. [23]

The voltammetric responses obtained during the 1st and 10th electropolymerization cycles of the WO_3@poly[1]_s and WO_3@poly[1]_r nanocomposite films are depicted in Figure 2 (a), along with the same electropolymerization cycles for the pristine poly[1], for comparison. The voltammetric profiles for the complete film electropolymerizations are shown in Figure S6 in SI and the peak potential values are summarized in Table S1.

Figure 2

The nanocomposite voltammetric responses for the electropolymerization are similar to those of pristine poly[1], but with small shifts of the anodic and cathodic peaks to more and less negative potentials, respectively. These results suggest that the presence

of the WO_3 NPs did not change the electropolymerization mechanism of poly[1]. Thus, the two peaks observed in the first anodic half-cycle at E_{pa} = 0.86-0.88 and 1.04-1.08 V are assigned to the [Ni(3-Mesalen)] monomer oxidation and subsequent formation of oligomers/polymer on the working electrode, while the two cathodic peaks in the reverse scan at E_{pc} = 0.20-0.21 and 0.69-0.70 V are attributed to the reduction of the as-formed nanocomposite films. The new anodic peak at E_{pa} = 0.42 V, in second and subsequent polymerization cycles, corresponds to the oxidation of the as-formed nanocomposite films [32,33,34].

The nanocomposite and pristine film voltammetric responses during redox cycling (5^{th} scan) in $LiClO_4/CH_3CN$ and $LiClO_4$/PC 0.1 mol dm^{-3}, are depicted in Figures 2 (b) and (c), respectively. The *i-E* curves obtained during the complete film conditioning process are shown in Figure S7; Tables S2 and S3 summarize the corresponding peak potential values.

The nanocomposites and pristine films have similar electrochemical responses in both supporting electrolytes. Generally, the peaks are less well defined in $LiClO_4$/PC than in $LiClO_4/CH_3CN$. Moreover, the nanocomposite voltammetric responses exhibit slightly higher current intensities when compared to those of the pristine film, which is attributed to a larger electroactive surface area of the as-prepared nanocomposite films, as result of the incorporation of WO_3 NPs in the polymeric matrix. This is in agreement with the determined electroactive surface coverages: Γ = 0.19 (± 0.02) μmol cm^{-2} for poly[1] and Γ = 0.22 and 0.27 (± 0.02) μmol cm^{-2} for WO_3@poly[1]_s and WO_3@poly[1]_r nanocomposites, respectively. The higher Γ values for WO_3@poly[1]_r suggest that the reflux step in methodology ii) may additionally promote the incorporation of higher amount of WO_3 NPs, as result of higher monomer adsorption onto nanoparticles surface when compared to methodology i), which only include the sonication step.

The visual inspection of the WO_3@poly[1] nanocomposite films during their redox switching confirm the similarity of their EC behaviour to the pristine poly[1] [34]. In Figure 2 (d), representative photographs of the WO_3@poly[1]_r film with distinct colours at different oxidation states are presented: yellow (E = 0.0 V), green (E = 0.7 V) and russet (reddish-brown) (E = 1.3 V).

3.3 Composition and morphology

Based on the evidence of the studies described in the previous sections, compositional and morphological characterization was focused on the WO_3@poly[1]_r nanocomposite, which has the advantage of higher electroactive surface coverage under given fabrication conditions.

Qualitatively, the XPS results for WO_3@poly[1]_r showed the presence of Ni, C, N and O from the pristine film, Cl from the supporting electrolyte (which also contributes to O and N contents), and W due to the incorporated WO_3 NPs (with which also contribute to O). The deconvoluted high-resolution XPS spectra of the nanocomposite in the C1s, N1s and W4f regions are depicted in Figures 3, 4 and 5, respectively, along with the spectra of poly[1], for comparison (C1s and N1s regions). The spectra in the O1s, Cl2p and Ni2p regions are shown in Figures S8, S9 and S10, respectively.

Figure 3

Figure 4

Figure 5

In the C1s region, the high-resolution spectra were deconvoluted into four peaks: (i) a main peak at 284.6 eV, attributed to aromatic and aliphatic carbons of the *salen*

ligand, (ii) a peak at 285.8-286.0 eV, assigned to carbon bound to oxygen or nitrogen of the *salen* moiety, (iii) a peak at 286.7-287.0 eV, ascribed to C≡N (from CH_3CN, Figure 3 (a), (a'), (b) and (b')) or to C=O (from PC, Figure 3 (c) and (c')), in both cases associated with solvent entrapped in the film, and (iv) a peak at 289.2-290.0 eV, assigned to a shake-up satellite associated with π-π* transitions in the aromatic carbon rings of the ligand [33,57]. The spectrum of the nanocomposite after redox switching in $LiClO_4$/PC (Figure 3 (c')) showed a slightly different profile, which can be attributed to the PC incorporation and consequent increase of carbon-oxygen bonds.

The N1s high-resolution spectra of films analysed before redox and after redox cycling in $LiClO_4/CH_3CN$ (Figure 4 (a), (a'), (b) and (b')) were deconvoluted into four peaks. The peaks at 399.3-399.5 eV and 400.2-400.4 eV are attributed to the nitrogen from ligand system (N=C and N-C bonds), the peak at higher energy, 401.2-401.5 eV, is assigned to the occluded CH_3CN (N≡C) [33] and the peak at 403.4-403.6 eV is attributed to a shake-up phenomenon [58]. The spectra of the films upon redox switching in $LiClO_4$/PC (Figure 4 (c) and (c')) showed equivalent peaks in the ranges 399.4-399.5 eV, 400.7 eV and 403.0-403.2 eV; when the solvent was changed to PC, the absence of the peak previously assigned to CH_3CN supports the interpretation.

The O1s spectra of pristine and nanocomposite films before redox switching (Figure S8 (a) and (a')) were deconvoluted into three peaks: a peak at 531.2 eV assigned to the oxygen from *salen* coordination sphere [33] and two other peaks at 532.4-532.6 eV and 533.3-533.4 eV attributed to occluded ClO_4^- with different local environments. In the nanocomposite spectrum, the peak at 531.2 eV also has the contribution of O-W bonds from WO_3 and the peaks at higher energy from the –OH groups, C=O and C-O bonds of WO_3 contaminants. The film O1s spectra after redox switching in $LiClO_4/CH_3CN$ (Figure S8 (b) and (b')) exhibit the same peak at 531.1-531.6 eV (O from *salen* coordination

sphere) [33] and one peak at 532.7-533.1 eV, assigned to occluded ClO_4^-, in higher amounts, due to charge compensation processes during the redox cycles [33]. Note that it is also expected the contribution of Li^+ ion in the oxidation charge compensation of poly[1] [34], but its content was not considered in the XPS analysis due to the low sensitivity of XPS instrument and consequent inaccurate Li %. After redox switching in $LiClO_4$/PC, the spectra of pristine poly[1] (Figure S8 (c)), besides the two peaks at 531.3 eV and 532.8 eV (similarly to redox switching in CH_3CN), also show an additional peak at 533.9 eV, assigned to oxygen-carbon bonds due to occluded PC [59]. In the spectra of WO_3@poly[1]_r after redox cycling in $LiClO_4$/PC (Figure S8 (c')) the three peaks at 531.1, 532.4 and 534.4 eV were also observed, together with another peak at 533.4 eV, assigned to ClO_4^- trapped in the polymeric film during its electrodeposition.

The high resolution Cl2p spectra (Figure S9) show peaks assigned to $Cl2p_{3/2}$ (207.8-208.2 eV) and $Cl2p_{1/2}$ (209.4-210.0 eV) and are consistent with the presence of ClO_4^- from supporting electrolyte occluded within the films. In the Ni2p region (Figure S10) the high resolution spectra are characteristic of Ni in a formal +2 oxidation state and the peaks can be assigned to the $Ni2p_{3/2}$ (855.1-855.4 eV), $Ni2p_{3/2}$ satellite (860.1-860.7 eV), $Ni2p_{1/2}$ (872.3-872.5 eV) and $Ni2p_{1/2}$ satellite (877.3-877.8 eV).

The deconvoluted spectrum of the nanocomposite film, Figure 5, in the W4f region exhibits two peaks at 36.1-36.2 eV and 38.2-38.4 eV, with a doublet separation of $\Delta \approx$ 2.20 eV, attributed to the $W^{(VI)}$ $4f_{7/2}$ and $W^{(VI)}$ $4f_{5/2}$ levels of the tungsten in WO_3 [49,54], similarly to the XPS data for free WO_3 NPs.

We now move from qualitative analysis (based on the peak energies) to quantitative analysis (based on peak areas). In Table 1 are summarized the surface atom percentages of all elements and the calculated surface atom ratios for films before and after redox switching in $LiClO_4/CH_3CN$ and $LiClO_4$/PC.

Table 1

Before redox switching, the nanocomposite film shows N/Ni, O/Ni and Cl/Ni atom ratios slightly larger than the expected values based on [Ni(3-Mesalen)] chemical structure ($N/Ni_{theoretical}$ = $O/Ni_{theoretical}$ = 2.0). CH_3CN trapped in the polymeric matrix during electropolymerization is the origin of the elevated N content. Trapped $LiClO_4$ is the origin of the high Cl content and, in part the high O content; the presence of WO_3 NPs also contributes to elevated O content.

After redox switching in $LiClO_4/CH_3CN$ and $LiClO_4$/PC the WO_3@poly[1]_r films show only slight increases in these atom ratios (most notably for the O/Ni ratio) when compared with the large increases observed for poly[1] in similar conditions. The increase in O, Cl and N contents after redox switching is explained by the accumulation of ClO_4^- and solvent inside film, as a consequence of the charge compensation/solvation processes, occurring during the course of several redox cycles [60,61]. For poly[1] submitted to redox switching in $LiClO_4$/PC, the increase in O/Ni and Cl/Ni is less noticeable than in $LiClO_4/CH_3CN$, indicating lesser incorporation of ClO_4^- with PC, as already observed [34]. The lower incorporation of ClO_4^- in nanocomposite in comparison to the pristine film can be explained by the presence of the WO_3 NPs, which disrupt the polymeric matrix packaging and thus facilitate both the ingress and the expulsion of supporting electrolyte.

The presence of W from the WO_3 NPs provides an indication of the successful preparation of the WO_3@poly[1]_r nanocomposite. Furthermore, the presence of W in films after redox switching indicates a stable composition of the nanocomposite as-prepared, with the WO_3 NPs remaining incorporated in the polymeric structure after the

potential cycling. Quantitative considerations here are less straightforward for a combination of materials and analytical reasons. First, the particle size (ca. 35 nm) is over an order of magnitude smaller than the film thickness (> 1000 nm, based on perfilometry studies), so the particles are likely to be fully enveloped in polymer. Second, XPS is highly surface sensitive, so the particles are less likely to be within the sampled volume.

Figure 6 depicts a representative SEM micrograph of the WO_3@poly[1]_r film and the respective EDS spectrum at a selected region, identified as Z1.

Figure 6

The micrograph shows a continuous layer with irregular surface, typical of the pristine poly[1] [34], over which are distinguished small fragments (region Z1). The analysis by EDS of these fragments (Figure 6 (b)) revealed that, beyond the compositional elements of the pristine film (C, O, Ni) and from the supporting electrolyte (Cl) and substrate (In), it was detected W, which corroborates the presence of WO_3 NPs occluded on Ni-*salen* polymeric matrix. The distinction between EDS and XPS is that the former samples more deeply into the material. A lower amplification SEM micrograph of the nanocomposite film, Figure S11 (a), allowed to observe an approximately homogeneous distribution of WO_3 as nanoclusters within the polymer film, which is confirmed by the elemental mapping images of Figure S11 (c)-(e)).

3.4 *In –situ* UV-Vis spectroscopy

In Figures 7 and 8 are depicted the absolute UV-Vis spectra acquired during the oxidation of the WO_3@poly[Ni(*salen*)] nanocomposites in $LiClO_4/CH_3CN$ and $LiClO_4$/PC, respectively; for comparison, the equivalent spectra for pristine poly[1] are

also depicted. The spectra obtained during film reduction showed an inverse behaviour; since these provide no additional information, they are omitted for simplicity.

Figure 7

Figure 8

The nanocomposite spectra show four electronic bands in both supporting electrolytes, similarly to the spectra of the pristine film. The electronic band profiles with the applied potential are most readily appreciated in the differential spectra, depicted using the responses at selected potentials as reference points (Figures S12 and S13), and by the representation of the absorbance vs. potential (*Abs* vs. *E*) profiles, at the wavelength of the detected bands (Figures 7 and 8 (a'), (b') and (c')). These representations revealed that the potential dependences of the electronic bands of the nanocomposite are similar to those of poly[1]: they show three main band profiles, characteristic of the pristine [34] and other similar poly[M(*salen*)] films [32,33].

The energies of the electronic bands are summarised in Table 2, as well as the molar extinction coefficients, ε, estimated from the slopes of *Abs* vs. *Q* plots (Figure S14 and S15) using Equation 1.

Table 2

Based on the rationale of ligand-based film oxidation, supported by the electronic bands ε-values and previously proposed for pristine [34] and other similar poly[M(*salen*)] films [32,33,62], the following band assignment can be made. First, the bands at λ = 325-327 nm are attributed to the intervalence transition (band gap, E_g = 3.79 eV for pristine

film and E_g = 3.81 / 3.82 eV for nanocomposites). Second, the bands at λ = 396-402 nm (3.09-3.13 eV) and λ = 826-852 nm (1.46-1.50 eV), that appear during the film oxidation, are attributed to transitions from the valence band to the antibonding and bonding polaron levels (or between polaron levels), respectively. Third, the bands at λ = 509-513 nm (2.42-2.44 eV), with their different *Abs* vs. *E* profiles, are assigned to charge transfer (CT) transitions between the metal and the oxidized ligand.

The data summarized in Table 2 reveal that the energies of the observed bands in nanocomposites are similar to those of the pristine film in the same supporting electrolyte, showing that the incorporation of WO_3 in poly[1] matrix did not change the metallopolymer electronic structure. The ε-values for the nanocomposite electronic bands are also similar to those of pristine film, except for the bands attributed to CT transitions at λ = 509-513 nm (2.42-2.44 eV) in $LiClO_4/CH_3CN$ and at λ = 509-510 nm (2.43-2.44 eV) in $LiClO_4$/PC. For the nanocomposites, the CT band ε-values decrease (by ca. 36 %) from $LiClO_4/CH_3CN$ to $LiClO_4$/PC electrolytes ($\varepsilon \approx 15.4 \times 10^3$ vs. 9.86×10^3 cm^{-1} mol^{-1} dm^3) similarly to pristine film and as reported previously [34]. Beyond that, the main achievement is that the ε-values of these bands are lower (by ca. 11 % in $LiClO_4/CH_3CN$ and by ca. 13 % in $LiClO_4$/PC) in the nanocomposite film than the pristine film. Specifically, in $LiClO_4/CH_3CN$, $\varepsilon = 17.27 \times 10^3$ cm^{-1} mol^{-1} dm^3 for poly[1], decreasing to $\varepsilon = 15.03 \times 10^3$ and 15.72×10^3 cm^{-1} mol^{-1} dm^3 for WO_3@poly[1]_s and WO_3@poly[1]_r, respectively. This decrease of the CT band ε-values for nanocomposite films is a good outcome since this CT band correlates with irreversible over-oxidation, i.e. decreased stability of poly-*salen* oxidised states. We thus anticipate increased film stability upon WO_3 NPs incorporation.

3.5 Electrochromic properties

The EC parameters - switching times, optical contrasts, changes of the optical density and colouration efficiencies - of WO_3@poly[1] nanocomposites were determined in order to evaluate the effect of WO_3 incorporation on the EC response of the material. The studies were performed with nanocomposite films prepared from the two different pre-treatment starting solutions (ultrasound or ultrasound + reflux) and in $LiClO_4/CH_3CN$ and $LiClO_4$/PC supporting electrolytes, to explore the effect of these conditions in the EC properties.

Figure 9 depicts representative chronoabsorptograms for nanocomposite and pristine polymer films (with electroactive coverages in the range Γ = 0.06-0.10 μmol cm^{-2}) in $LiClO_4/CH_3CN$ supporting electrolyte, considering the colour change between yellow (E = 0.0 V) and green (E = 0.7 V), at fixed λ=750 nm; the equivalent results obtained in $LiClO_4$/PC are depicted in Figure S16.

Figure 9

The measured nanocomposite switching times were in the range τ = 1.3 - 5.4 s in $LiClO_4/CH_3CN$ and τ = 5.4 - 8.1 s in $LiClO_4$/PC; higher switching times in $LiClO_4$/PC were previously noted for pristine films [34]. In $LiClO_4/CH_3CN$ medium, the nanocomposites showed significantly shorter switching times, by 33 % for WO_3@poly[1]_s and by 46 % for WO_3@poly[1]_r, than the corresponding pristine film; WO_3 incorporation is clearly advantageous. In $LiClO_4$/PC, the nanocomposite switching times show only modest or no improvement over those of the pristine film.

Table 3 summarises the optical contrasts, changes in optical density, charge requirements and colouration efficiencies, determined from the chronoabsorptograms considering the full optical change. In $LiClO_4/CH_3CN$, the ΔT increased from

ΔT = 18.7 % in the pristine film to $\Delta T \approx$ 31.0 % in the nanocomposites (an improvement of ca. 40 %), whereas in $LiClO_4$/PC, ΔT for the nanocomposites remains similar or slight decreases in comparison with the poly[1] film.

Table 3

Each polymeric film shows similar ΔOD values in both supporting electrolytes. Nonetheless, ΔOD values slightly decrease from ΔOD ≈ 0.40 in pristine film to ΔOD ≈ 0.33 (average value) in nanocomposites.

The colouration efficiency, which effectively normalises for population, increases in $LiClO_4/CH_3CN$ from η = 90.0 $cm^2\ C^{-1}$ for pristine film to η = 115.2 $cm^2\ C^{-1}$ for WO_3@poly[1]_s (+ 22 %) and η = 103.6 $cm^2\ C^{-1}$ for WO_3@poly[1]_r (+ 13 %), which indicates a greater power efficiency of the nanocomposite films. In $LiClO_4$/PC, the η-values obtained for nanocomposites films remain similar to the pristine film (range between η = 81.6-85.9 $cm^2\ C^{-1}$), with the decrease of charge requirements being less significant for nanocomposites in this electrolyte. The enhancement observed in some EC properties for nanocomposites can be explained by the better charge carrier transport due to the organized network structure provided by the WO_3 NPs, which can act as a "freeway" for the charge carriers [29]. The new nanoarchitecture, provided by the WO_3 NPs incorporation, probably decrease the poly[1] film packaging and favour the supporting electrolyte movement inside the film structure allowing a faster electrochromic response (in $LiClO_4/CH_3CN$). This is in agreement with the higher electroactive surface coverage obtained for WO_3@poly[1]_r (larger amount of WO_3 NPs incorporated) and justify the faster response times for this nanocomposite compared to WO_3@poly[1]_s. The minor differences between the EC parameters of both type of

nanocomposites (optical contrast, charge requirements and colouration efficiencies) are attributed to the experimental uncertainty.

The electrochemical stability was evaluated using representative thick pristine (Γ = 0.19 μmol cm^{-2}) and WO_3@poly[1]_r nanocomposite (Γ = 0.27 μmol cm^{-2}) films by chronoamperometry, during around 10 000 redox cycles in 0.1 mol dm^{-3} $LiClO_4$/PC. This supporting electrolyte was chosen because its low volatility as previously shown for pristine film [34]. The thick films were chosen for the electrochemical stability tests since it is in this type of films that problems associated with ionic and electronic conduction become more significant.

The chronoamperograms are depicted in Figure S17 (a) in SI. The switching times are similar for both the thick films used in these studies : τ = 19 - 22 s for poly[1] and τ = 17 - 23 s for WO_3@poly[1]_r (measured considering 90 % of the total current intensity change in 0.1 mol dm^{-3} $LiClO_4$/PC).

The data revealed that the thick nanocomposite has a lower electrochemical stability than the analogous pristine film (29.6 % vs. 13.7 % of charge loss); expressed differently, its short term performance is enhanced, but with some sacrifice of stability. We speculate that the lowest electrochemical stability maybe due to some WO_3 NPs leaching during the ingress/egress of counter-balancing ions and supporting electrolyte during the several redox cycles, which may cause the film nanoarchitecture damage by collapsing the polymer matrix. A SEM micrograph of WO_3@poly[1]_r after the 10 000 electrochemical cycles (Figure S17 (b)), corroborates this assumption, showing clearly the damaged structure of the thick nanocomposite film.

4. CONCLUSIONS

The results showed that poly[1] was successfully electropolymerized in the presence of WO_3 NPs, previously prepared and characterized by XRD, XPS and FTIR. These techniques confirmed the preparation of quasi-spherical WO_3 nanoparticles with a monoclinic structure, high degree of crystallinity and sizes of ≈ 38 or 35 nm (SEM or TEM, respectively), similar to those estimated by XRD ≈ 30 - 40 nm.

The resultant nanocomposite films showed similar electrochemical responses to the pristine film, but with higher electroactive surface coverages, indicating an advantage of the polymeric nanocomposite assemblage. SEM and XPS confirmed the presence of WO_3 NPs on the poly[1] matrix. Furthermore, the XPS analysis revealed that the redox processes promotes the accumulation of large amounts of supporting electrolyte (due to charge compensation processes) in the polymeric matrix, although to a lesser extent for the nanocomposite film. UV-Vis spectroscopic data showed that the electronic bands of nanocomposite films have similar profiles and energies to those of poly[1], confirming the maintenance of the pristine film electronic structure. Lower ε-values for the nanocomposite CT bands revealed greater stability of the composite to over-oxidation.

The nanocomposite films showed more favorable EC properties in $LiClO_4/CH_3CN$ than the pristine film, with lower switching times (ranging between τ = 1.3 and 3.6 s), higher optical contrasts (ΔT ≈ 31 %) and better colouration efficiencies (η = 103.6 and 115.2 $cm^2\ C^{-1}$ for WO_3@poly[1]_r and WO_3@poly[1]_s, respectively). In overview, these results revealed the advantage of the preparation of the nanocomposite with WO_3 NPs in order to surpass the EC performance of the pristine poly[1]. Furthermore, the methodology ii), adopted for the preparation of the nanocomposite polymerization solutions and that involved the reflux step, showed to be highly beneficial for the final nanocomposite EC response times (in $LiClO_4/CH_3CN$).

ACKNOWLEDGMENTS

The work was funded by European Union and Fundação para a Ciência e a Tecnologia (FCT)/MEC under FEDER funds (POCI/01/0145/FEDER/007265) and Program PT2020 (UID/QUI/50006/2013). MN thanks FEDER funds POCI/01/0145/FEDER/007265 and PT2020 UID/QUI/50006/2013 for her post-doctoral grant.

REFERENCES

[1] C.K. Chiang, C.R. Fincher, Y.W. Park, A.J. Heeger, H. Shirakawa, E.J. Louis, S.C. Gau, A.G. MacDiarmid, Electrical Conductivity in Doped Polyacetylene, Phys. Rev. Lett. 39 (1977) 1098-1101.

[2] H. Shirakawa, E.J. Louis, A.G. MacDiarmid, C.K. Chiang, A.J. Heeger, Synthesis of Electrically Conducting Organic Polymers - Halogen Derivatives of Polyacetylene, (CH)X, Chem. Soc., Chem. Commun. (1977) 578-580.

[3] Y.J. Ding, M.A. Invernale, D.M.D. Mamangun, A. Kumar, G.A. Sotzing, A Simple, Low Waste and Versatile Procedure to Make Polymer Electrochromic Devices, J. Mater. Chem. 21 (2011) 11873-11878.

[4] P. Pascariu, A. Airinei, M. Grigoras, L. Vacareanu, F. Iacomi, Metal-Polymer Nanocomposites Based on Ni Nanoparticles and Polythiophene Obtained by Electrochemical Method, Appl. Surf. Sci. 352 (2015) 95-102.

[5] F.J. Guo, H.Y. Mi, J.P. Zhou, Z.B. Zhao, J.S. Qiu, Hybrid Pseudocapacitor Materials From Polyaniline@Multi-Walled Carbon Nanotube With Ultrafine Nanofiber-Assembled Network Shell, Carbon 95 (2015) 323-329.

[6] S. Abdulla, T.L. Mathew, B. Pullithadathil, Highly Sensitive, Room Temperature Gas Sensor Based on Polyaniline-Multiwalled Carbon Nanotubes (PANI/MWCNTs) Nanocomposite for Trace-Level Ammonia Detection, Sens. Actuator B-Chem 221 (2015) 1523-1534.

[7] F.A. Rafiqi, K. Majid, Synthesis, Characterization, Luminescence Properties and Thermal Studies of Polyaniline and Polythiophene Composites With Rare Earth Terbium(III) Complex, Synth. Met. 202 (2015) 147-156.

[8] C. Janaky, N.R. de Tacconi, W. Chanmanee, K. Rajeshwar, Electrodeposited Polyaniline in a Nanoporous WO_3 Matrix: an Organic/Inorganic Hybrid Exhibiting Both p- and n-Type Photoelectrochemical Activity, Phys. Chem. C 116 (2012) 4234-4242.

[9] J.H. Zhu, S.Y. Wei, L. Zhang, Y.B. Mao, J. Ryu, P. Mayinakuli, A.B. Karki, D.P. Young, Z.H. Guo, Conductive Polypyrrole/Tungsten Oxide Metacomposites with Negative Permittivity, Phys. Chem. C 114 (2010) 16335-16342.

[10] D.Y. Ma, G.Y. Shi, H.Z. Wang, Q.H. Zhang, Y.G. Li, Controllable Growth of High-Quality Metal Oxide/Conducting Polymer Hierarchical Nanoarrays with Outstanding Electrochromic Properties and Solar-Heat Shielding Ability, J. Mater. Chem. A 2 (2014) 13541-13549.

[11] S.J. Moon, E. Baranoff, S.M. Zakeeruddin, C.Y. Yeh, E.W.G. Diau, M. Gratzel, K. Sivula, Enhanced Light Harvesting in Mesoporous TiO_2/P_3HT Hybrid Solar Cells Using a Porphyrin Dye, Chem. Commun. 47 (2011) 8244-8246.

[12] J.H. Heo, S.H. Im, J.H. Noh, T.N. Mandal, C.S. Lim, J.A. Chang, Y.H. Lee, H.J. Kim, A. Sarkar, M.K. Nazeeruddin, M. Gratzel, S.I. Seok, Efficient Inorganic-Organic Hybrid Heterojunction Solar Cells Containing Perovskite Compound and Polymeric Hole Conductors, Nat. Photonics 7 (2013) 487-492.

[13] D. Hidalgo, S. Bocchini, M. Fontana, G. Saracco, S. Hernandez, Green and Low-Cost Synthesis of PANI-TiO_2 Nanocomposite Mesoporous Films for Photoelectrochemical Water Splitting, RSC Adv. 5 (2015) 49429-49438.

[14] R. Jain, D.C. Tiwari, P. Karolia, Highly Sensitive and Selective Polyaniline-Zinc Oxide Nanocomposite Sensor for Betahistine Hydrochloride in Solubilized System, J. Mol. Liq. 196 (2014) 308-313.

[15] L. Chen, Z.X. Song, G.C. Liu, J.S. Qiu, C. Yu, J.W. Qin, L. Ma, F.Q. Tian, W. Liu, Synthesis and Electrochemical Performance of Polyaniline-MnO_2 Nanowire Composites for Supercapacitors, J. Phys. Chem. Solids 74 (2013) 360-365.

[16] S.M. Hicks, A.J. Killard, Electrochemical Impedance Characterisation of Tungsten Trioxide-Polyaniline Nanocomposites for Room Temperature Acetone Sensing, Sens. Actuator B-Chem. 194 (2014) 283-289.

[17] P.G. Su, Y.T. Peng, Fabrication of a Room-Temperature H_2S Gas Sensor Based on PPy/WO_3 Nanocomposite Films by In-Situ Photopolymerization, Sens. Actuator B-Chem. 193 (2014) 637-643.

[18] A.T. Mane, S.T. Navale, V.B. Patil, Room Temperature NO_2 Gas Sensing Properties of DBSA Doped PPy-WO_3 Hybrid Nanocomposite Sensor, Org. Electron. 19 (2015) 15-25.

[19] B.X. Zou, X.X. Liu, D. Diamond, K.T. Lau, Electrochemical Synthesis of WO_3/PANI Composite for Electrocatalytic Reduction of Iodate, Electrochim. Acta 55 (2010) 3915-3920.

[20] B.X. Zou, Y. Liang, X.X. Liu, D. Diamond, K.T. Lau, Electrodeposition and Pseudocapacitive Properties of Tungsten Oxide/Polyaniline Composite, J. Power Sources 196 (2011) 4842-4848.

[21] P.H. Yang, P. Sun, Z.S. Chai, L.H. Huang, X. Cai, S.Z. Tan, J.H. Song, W.J. Mai, Large-Scale Fabrication of Pseudocapacitive Glass Windows that Combine Electrochromism and Energy Storage, Angew. Chem.-Int. Edit. 53 (2014) 11935-11939.

[22] R. Sydam, M. Deepa, S.M. Shivaprasad, A.K. Srivastava, A WO_3-Poly(Butyl Viologen) Layer-by-Layer Film/Ruthenium Purple Film Based Electrochromic Device Switching by 1 Volt Application, Sol. Energy Mater. Sol. Cells 132 (2015) 148-161.

[23] H.G. Wei, X.R. Yan, S.J. Wu, Z.P. Luo, S.Y. Wei, Z.H. Guo, Electropolymerized Polyaniline Stabilized Tungsten Oxide Nanocomposite Films: Electrochromic Behavior and Electrochemical Energy Storage, J. Phys. Chem. C 116 (2012) 25052-25064.

[24] A.C. Nwanya, C.J. Jafta, P.M. Ejikeme, P.E. Ugwuoke, M.V. Reddy, R.U. Osuji, K.I. Ozoemena, F.I. Ezema, Electrochromic and Electrochemical Capacitive Properties of Tungsten Oxide and Its Polyaniline Nanocomposite Films Obtained by Chemical Bath Deposition Method, Electrochim. Acta 128 (2014) 218-225.

[25] G.F. Cai, J.P. Tu, D. Zhou, J.H. Zhang, X.L. Wang, C.D. Gu, Dual Electrochromic Film Based on WO_3/Polyaniline Core/Shell Nanowire Array, Sol. Energy Mater. Sol. Cells 122 (2014) 51-58.

[26] J. Zhang, J.P. Tu, D. Zhang, Y.Q. Qiao, X.H. Xia, X.L. Wang, C.D. Gu, Multicolor Electrochromic Polyaniline-WO_3 Hybrid Thin Films: One-Pot Molecular Assembling Synthesis, J. Mater. Chem. 21 (2011) 17316-17324.

[27] J. Zhang, J.P. Tu, G.H. Du, Z.M. Dong, Y.S. Wu, L. Chang, D. Xie, G.F. Cai, X.L. Wang, Ultra-Thin WO_3 Nanorod Embedded Polyaniline Composite Thin Film: Synthesis and Electrochromic Characteristics, Sol. Energy Mater. Sol. Cells 114 (2013) 31-37.

[28] C. Dulgerbaki, A.U. Oksuz, Efficient Electrochromic Materials Based on PEDOT/WO_3 Composites Synthesized in Ionic Liquid Media, Electroanalysis 26 (2014) 2501-2512.

[29] C. Janaky, K. Rajeshwar, The Role of (Photo)electrochemistry in the Rational Design of Hybrid Conducting Polymer/Semiconductor Assemblies: From Fundamental Concepts to Practical Applications, Prog. Polym. Sci. 43 (2015) 96-135.

[30] C. Pinheiro, A.J. Parola, F. Pina, J. Fonseca, C. Freire, Electrocolorimetry of Electrochromic Materials on Flexible ITO Electrodes, Sol. Energy Mater. Sol. Cells 92 (2008) 980-985.

[31] A. Branco, C. Pinheiro, J. Fonseca, J. Tedim, A. Carneiro, A.J. Parola, C. Freire, F. Pina, Solid-State Electrochromic Cells Based on M(*salen*)-Derived Electroactive Polymer Films, Electrochem. Solid State Lett. 13 (2010) J114-J118.

[32] J. Tedim, S. Patricio, J. Fonseca, A.L. Magalhaes, C. Moura, A.R. Hillman, C. Freire, Modulating Spectroelectrochemical Properties of Ni(*salen*) Polymeric Films at Molecular Level, Synth. Met. 161 (2011) 680-691.

[33] J. Fonseca, J. Tedim, K. Biernacki, A.L. Magalhaes, S.J. Gurman, C. Freire, A.R. Hillman, Structural and Electrochemical Characterisation of Pd(*salen*)-type Conducting Polymer Films, Electrochim. Acta 55 (2010) 7726-7736. ESTE PODE MANTER

[34] M. Nunes, M. Araujo, J. Fonseca, C. Moura, R. Hillman, C. Freire, High-Performance Electrochromic Devices Based on Poly Ni(*salen*)-Type Polymer Films, ACS Appl. Mater. Interfaces 8 (2016) 14231-14243.

[35] C. Janaky, N.R. de Tacconi, W. Chanmanee, K. Rajeshwar, Bringing Conjugated Polymers and Oxide Nanoarchitectures into Intimate Contact: Light-Induced Electrodeposition of Polypyrrole and Polyaniline on Nanoporous WO_3 or TiO_2 Nanotube Array, J. Phys. Chem. C 116 (2012) 19145-19155.

[36] C. Freire, B. de Castro, Spectroscopic Characterisation of Electrogenerated Nickel(III) Species. Complexes with N_2O_2 Schiff-Base Ligands Derived From Salicylaldehyde, J. Chem. Soc.-Dalton Trans. (1998) 1491-1497.

[37] A. Le Bail, H. Duroy, J.L. Fourquet, Ab-Initio Structure Determination of $LiSbWO_6$ by X-Ray Powder Diffraction, Mat. Res. Bull. 23 (1988) 447-452.

[38] S. Pokhrel, J. Birkenstock, M. Schowalter, A. Rosenauer, L. Mädler, Growth of Ultrafine Single Crystalline WO_3 Nanoparticles Using Flame Spray Pyrolysis, Crystal Growth & Design 10 (2010) 632-639.

[39] M. Deepa, R. Sharma, A. Basu, S.A. Agnihotry, Effect of Oxalic Acid Dihydrate on Optical and Electrochemical Properties of Sol-Gel Derived Amorphous Electrochromic WO_3 Films, Electrochim. Acta 50 (2005) 3545-3555.

[40] X.L. Sun, H.T. Cao, Z.M. Liu, J.Z. Li, Influence of Annealing Temperature on Microstructure and Optical Properties of Sol-Gel Derived Tungsten Oxide Films, Appl. Surf. Sci. 255 (2009) 8629-8633.

[41] J. Tedim, F. Gonçalves, M.F.R. Pereira, J.L. Figueiredo, C. Moura, C. Freire, A.R. Hillman, Preparation and Characterization of Poly[Ni(salen)(crown receptor)]/multi-walled carbon nanotube composite films, Electrochim. Acta 53 (2008) 6722-6731.

[42] M. Vilas-Boas, C. Freire, B. de Castro, A. R. Hillman, Electrochemical Characterization of a Novel Salen-Type Modified Electrode, J. Phys. Chem. B 102 (1998) 8533 - 8540.

[43] S.M. Dale, A. Glidle, A.R. Hillman, Spectroelectrochemical Observation of Poly(Benzo-c-Thiophene) n-doping and p-doping, J. Mater. Chem. 2 (1992) 99-104.

[44] M. Schott, H. Lorrmann, W. Szczerba, M. Beck, D.G. Kurth, State-of-the-Art Electrochromic Materials Based on Metallo-Supramolecular Polymers, Sol. Energy Mater. Sol. Cells 126 (2014) 68-73.

[45] P.M. Beaujuge, J.R. Reynolds, Color Control in π-Conjugated Organic Polymers for Use in Electrochromic Devices, Chem. Rev. 110 (2010) 268-320.

[46] C.M. Amb, A.L. Dyer, J.R. Reynolds, Navigating the Color Palette of Solution-Processable Electrochromic Polymers, Chem. Mat. 23 (2011) 397-415.

[47] T.Y. Wu, J.W. Liao, C.Y. Chen, Electrochemical Synthesis, Characterization and Electrochromic Properties of Indan and 1,3-Benzodioxole-Based Poly(2,5-Dithienylpyrrole) Derivatives, Electrochim. Acta 150 (2014) 245-262.

[48] G. Dawson, W.Z. Zhou, R. Blackley, Accelerated Electron Beam Induced Breakdown of Commercial WO_3 Into Nanorods in the Presence of Triethylamine, Phys. Chem. Chem. Phys. 13 (2011) 20923-20926.

[49] L.M. Bertus, C. Faure, A. Danine, C. Labrugere, G. Campet, A. Rougier, A. Duta, Synthesis and Characterization of WO_3 Thin Films by Surfactant Assisted Spray Pyrolysis for Electrochromic Applications, Mater. Chem. Phys. 140 (2013) 49-59.

[50] C. Costa, C. Pinheiro, I. Henriques, C.A.T. Laia, Inkjet Printing of Sol-Gel Synthesized Hydrated Tungsten Oxide Nanoparticles for Flexible Electrochromic Devices, ACS Appl. Mater. Interfaces 4 (2012) 1330-1340.

[51] X.X. Zou, G.D. Li, P.P. Wang, J. Su, J. Zhao, L.J. Zhou, Y.N. Wang, J.S. Chen, A Precursor Route to Single-Crystalline WO_3 Nanoplates with an Uneven Surface and Enhanced Sensing Properties, Dalton Trans. 41 (2012) 9773-9780.

[52] G. Socrates, *"Infrared and Raman Characteristic Group Frequencies - Tables and Charts"*; third ed.; John Wiley & Sons, Ltd.: England (2004).

[53] Z.C. Meng, A. Fujii, T. Hashishin, N. Wada, T. Sanada, J. Tamaki, K. Kojima, H. Haneoka, T. Suzuki, Morphological and Crystal Structural Control of Tungsten Trioxide for Highly Sensitive NO_2 Gas Sensors, J. Mater. Chem. C 3 (2015) 1134-1141.

[54] Z.X. Cai, H.Y. Li, X.N. Yang, X. Guo, NO Sensing by Single Crystalline WO_3 Nanowires, Sens. Actuator B-Chem. 219 (2015) 346-353.

[55] J. Zhu, W.Z. Li, J. Li, Y.M. Li, H.S. Hu, Y.H. Yang, Photoelectrochemical Activity of $NiWO_4/WO_3$ Heterojunction Photoanode Under Visible Light Irradiation, Electrochim. Acta 112 (2013) 191-198.

[56] S. Salmaoui, F. Sediri, N. Gharbi, C. Perruchot, S. Aeiyach, I.A. Rutkowska, P.J. Kulesza, M. Jouini, Hexagonal Nanorods of Tungsten Trioxide: Synthesis, Structure, Electrochemical Properties and Activity as Supporting Material in Electrocatalysis, Appl. Surf. Sci. 257 (2011) 8223-8229.

[57] N.M.D. Brown, J.A. Hewitt, B.J. Meenan, X-Ray-Induced Beam Damage Observed During X-Ray Photoelectron-Spectroscopy (XPS) Studies of Palladium Electrode Ink Materials, Surf. Interface Anal. 18 (1992) 187-198.

[58] A.I. Goldman, *X-Ray Techniques. Characterization of Materials.*; Wiley (2002).

[59] L.T. Weng, C. Poleunis, P. Bertrand, V. Carlier, M. Sclavons, P. Franquinet, R. Legras, Sizing Removal and Functionalization of the Carbon-Fiber Surface Studied by Combined TOF SIMS and XPS, J. Adhes. Sci. Technol. 9 (1995) 859-871.

[60] S. Bruckenstein, K. Brzezinska, A.R. Hillman, EQCM Studies of Polypyrrole Films. 1. Exposure to Aqueous Sodium Tosylate Solutions Under Thermodynamically Permselective Conditions, Electrochim. Acta 45 (2000) 3801-3811.

[61] S. Bruckenstein, K. Brzezinska, A.R. Hillman, EQCM Studies of Polypyrrole Films. Part 2. Exposure to Aqueous Sodium Tosylate Solutions Under Thermodynamically Non-Permselective Conditions, Phys. Chem. Chem. Phys. 2 (2000) 1221-1229.

[62] M. Vilas-Boas, C. Freire, B. de Castro, P.A. Christensen, A.R. Hillman, Spectroelectrochemical Characterisation of Poly[Ni(saltMe)]-Modified Electrodes, Chem.-Eur. J. 7 (2001) 139-150.

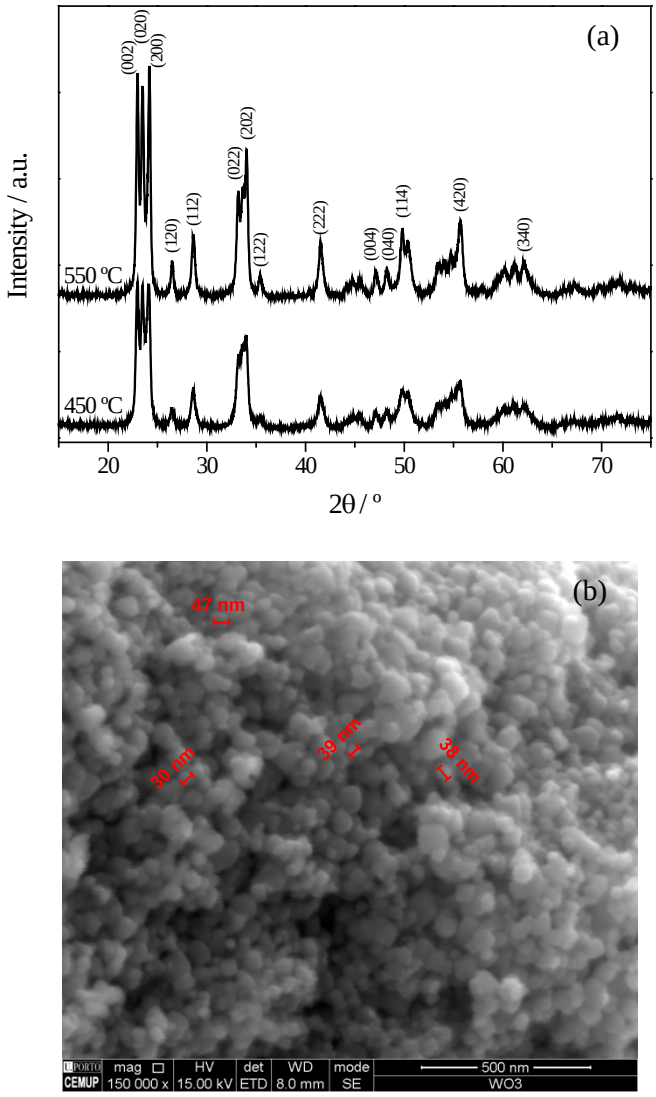

Figure 1. (a) XRD patterns of WO_3 NPs annealed at 450 and 550 ºC and (b) SEM micrographs of WO_3 NPs annealed at 550 ºC.

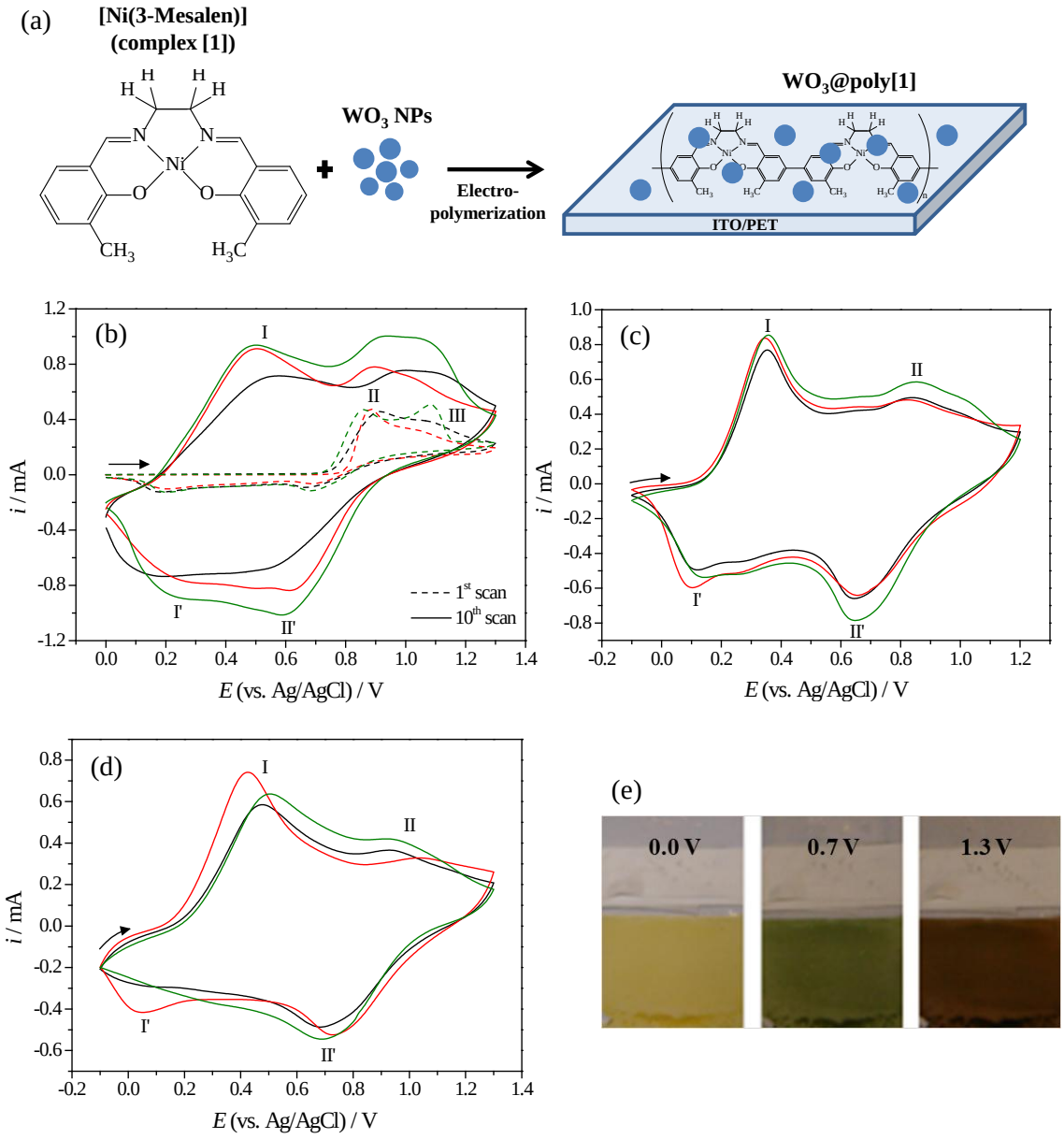

Figure 2. (a) Schematic representation of the complex [1] electropolymerization in the presence of WO_3 NPs. Cyclic voltammograms obtained during (b) the 1st and 10th scans of electrodeposition, (c) 5th scan of film redox switching in $LiClO_4/CH_3CN$, and (d) 5th scan of film redox switching in $LiClO_4$/PC for: poly[1] (—, Γ = 0.19 μmol cm^{-2}), WO_3@poly[1]_s (—, Γ = 0.22 μmol cm^{-2}) and WO_3@poly[1]_r (—, Γ = 0.27 μmol cm^{-2}); (e) representative photographs of WO_3@poly[1]_r in different oxidation states (*ex situ*, after emersion at potentials E = 0.0, 0.7 and 1.3 V).

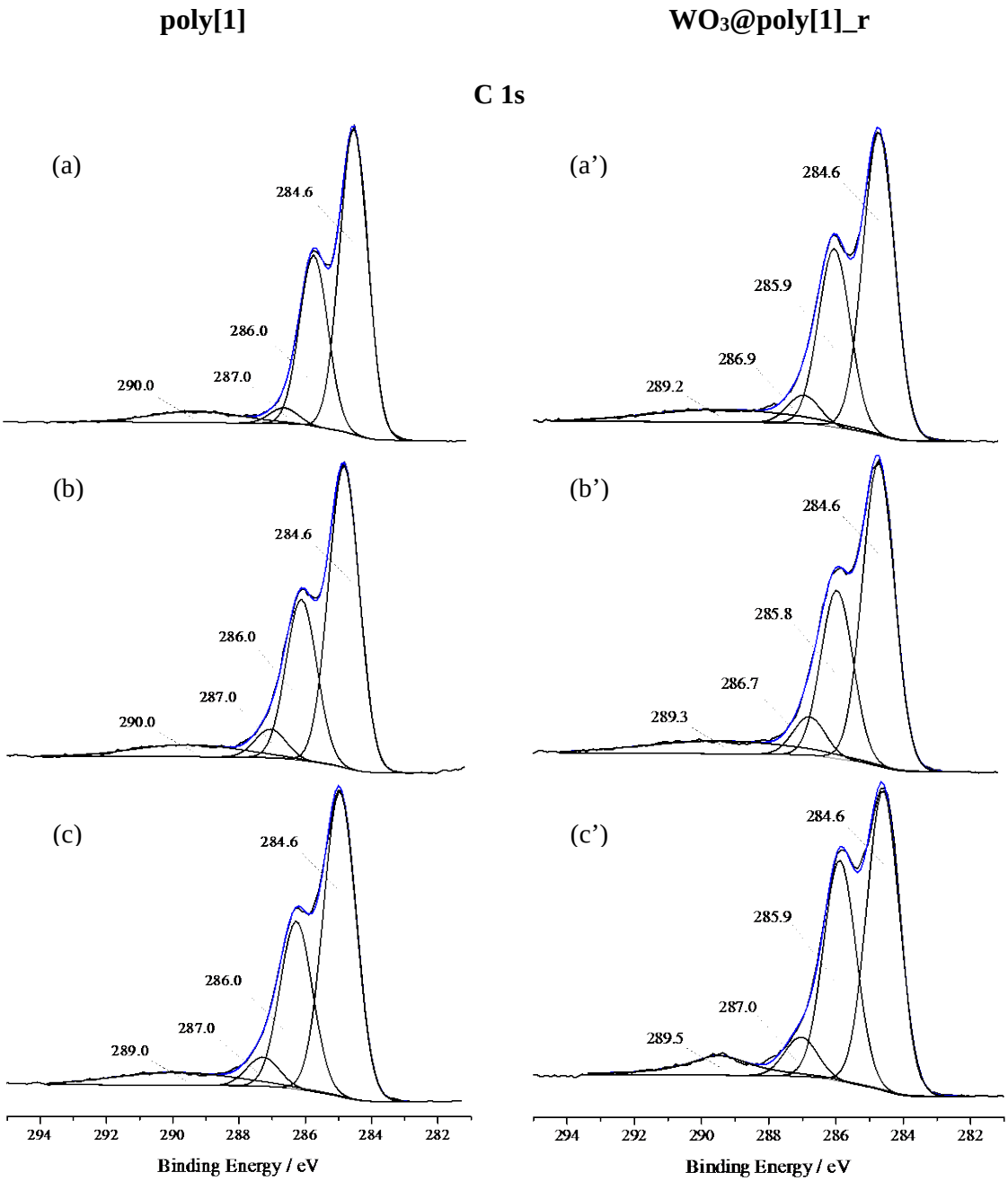

Figure 3. High-resolution XPS spectra of pristine poly[1] and WO_3@poly[1]_r in C1s region, with the corresponding deconvolutions, (a and a') before and after redox switching in (b and b') $LiClO_4/CH_3CN$ and (c and c') $LiClO_4$/PC.

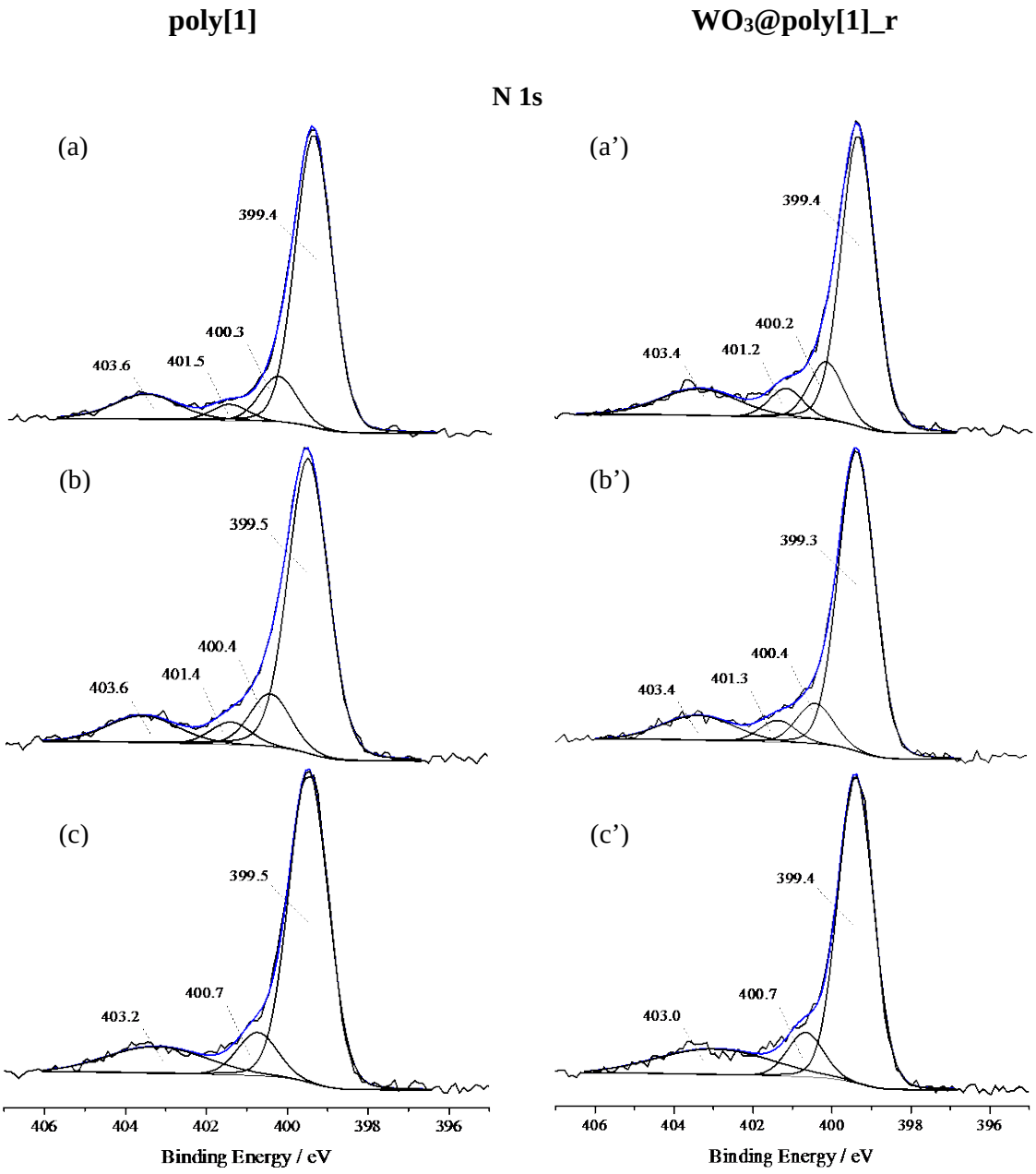

Figure 4. High-resolution XPS spectra of pristine poly[1] and WO_3@poly[1]_r in N1s region, with the corresponding deconvolutions, (a and a') before and after redox switching in (b and b') $LiClO_4/CH_3CN$ and (c and c') $LiClO_4$/PC.

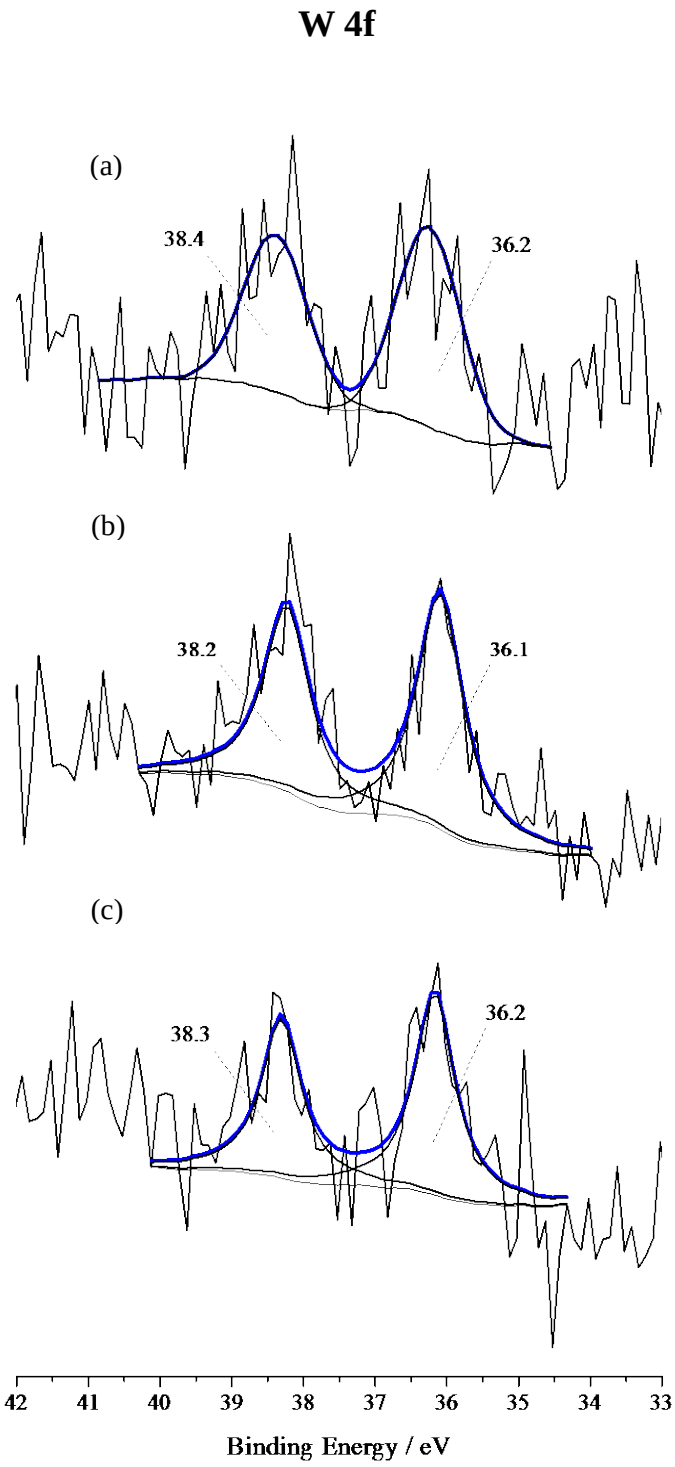

Figure 5. High-resolution XPS spectra of WO_3@poly[1]_r in W4f region, with the corresponding deconvolutions, (a) before and after redox switching in (b) $LiClO_4/CH_3CN$ and (c) $LiClO_4$/PC.

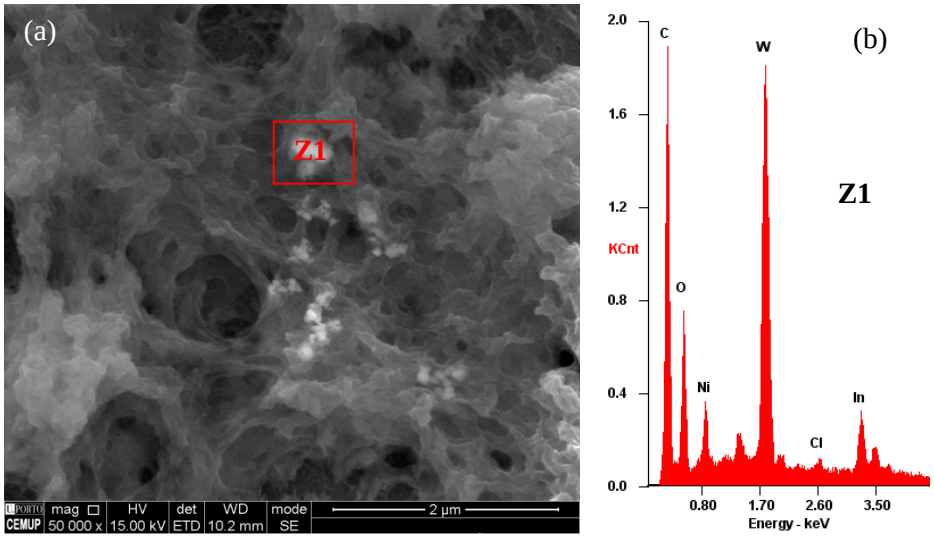

Figure 6. (a) Scanning electron micrograph and (b) respective EDS spectrum of WO_3@poly[1]_r film.

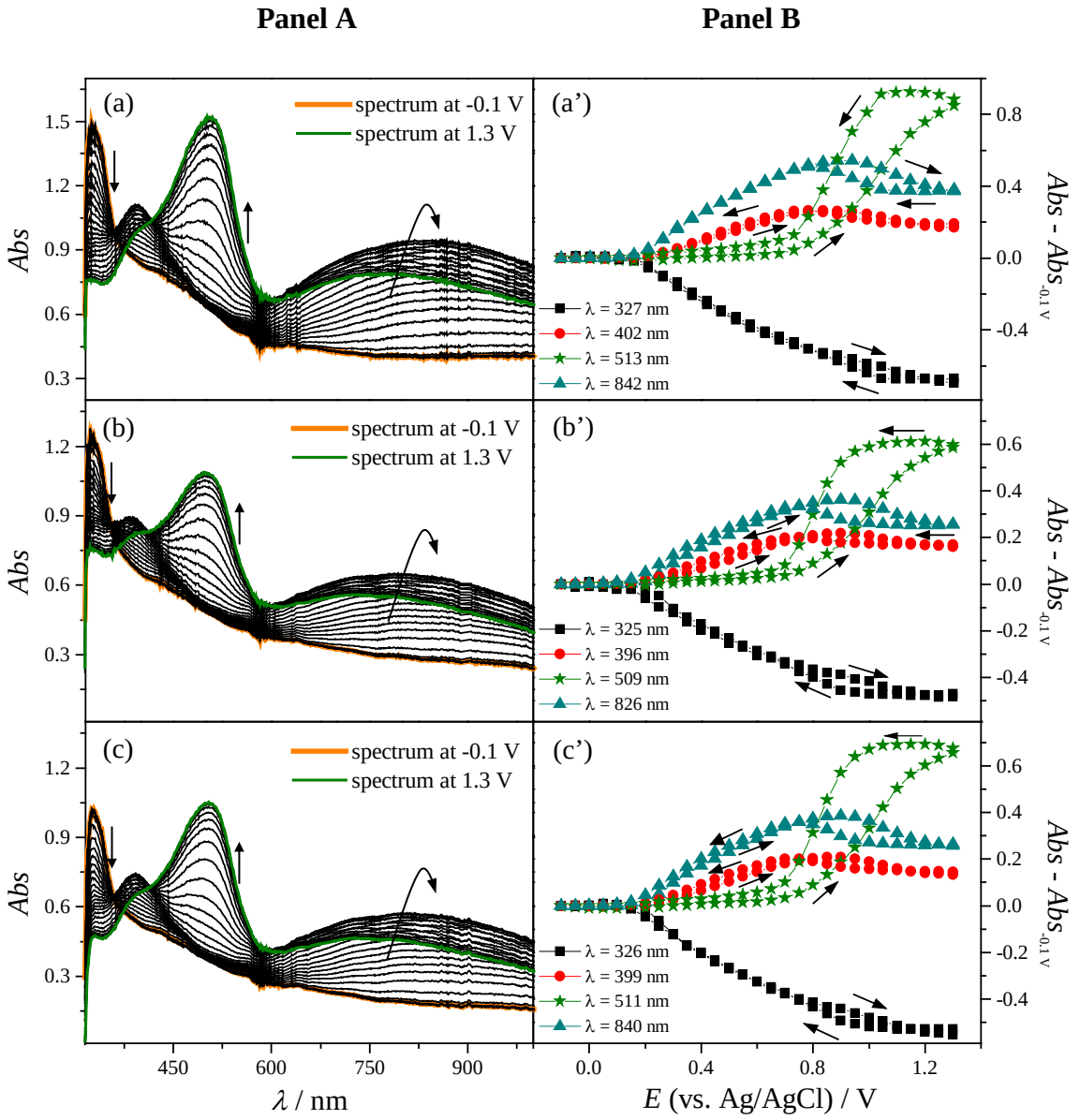

Figure 7. Panel A: Absolute UV-Vis spectra of (a) poly[1], (b) WO_3@poly[1]_s and (c) WO_3@poly[1]_r films acquired during films oxidation in 0.1 mol dm^{-3} $LiClO_4/CH_3CN$ (referenced to the electrolyte spectrum; Γ = 0.06-0.10 μmol cm^{-2}). Panel B: *Abs* vs. *E* plots for the electronic bands identified in absolute UV-Vis spectra, referenced to the spectra at *E* = -0.1 V (arrows indicate scan direction).

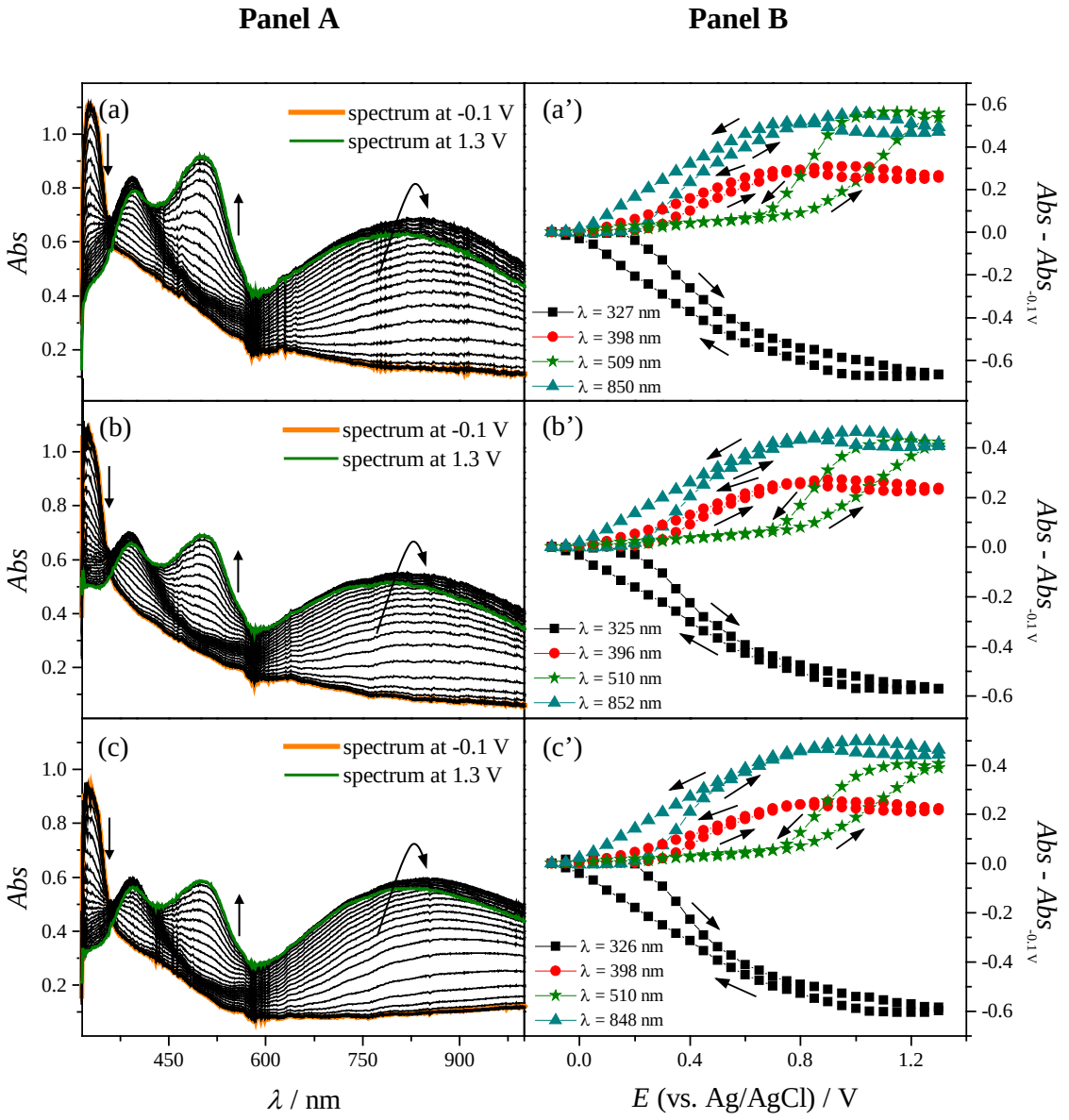

Figure 8. Panel A: Absolute UV-Vis spectra of (a) poly[1], (b) WO_3@poly[1]_s and (c) WO_3@poly[1]_r films acquired during films oxidation in 0.1 mol dm^{-3} $LiClO_4$/PC (referenced to the electrolyte spectrum; Γ = 0.06-0.10 μmol cm^{-2}). Panel B: *Abs* vs. *E* plots for the electronic bands identified in absolute UV-Vis spectra, referenced to the spectra at *E* = -0.1 V (arrows indicate scan direction).

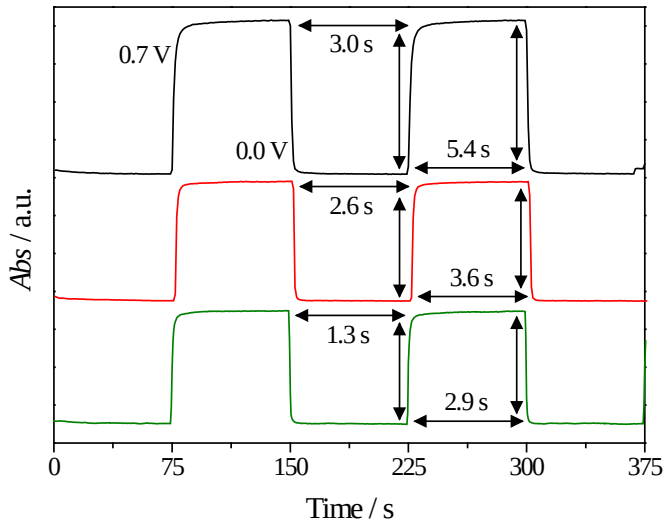

Figure 9. Chronoabsorptograms obtained for pristine (—), WO_3@poly[1]_s (—) and WO_3@poly[1]_r (—) films, at the fixed wavelength of λ=750 nm in 0.1 mol dm^{-3} $LiClO_4/CH_3CN$, indicating the measured switching times; *E* = 0.0 V (yellow) or 0.7 V (green), Γ = 0.06-0.10 μmol cm^{-2}.

TABLES

Table 1: XPS surface atom percentages and atom ratios of relevant elements for poly[1] and WO_3@poly[1]_r nanocomposite films, in their reduced states (E = 0.0 V).

Sample	Surface atom %						Surface atom ratio		
	Ni	C	N	O	Cl	W	N/Ni	O/Ni	Cl/Ni
poly[1]									
Before redox	3.5	75.5	7.6	12.0	1.3	-	2.2	3.4	0.4
After redox in CH_3CN	2.5	64.8	6.4	22.4	3.9	-	2.6	9.0	1.6
After redox in PC	2.7	72.8	6.6	15.9	2.1	-	2.4	5.9	0.8
WO_3@poly[1]_r									
Before redox	3.5	76.9	8.0	10.6	1.0	0.01	2.3	3.0	0.3
After redox in CH_3CN	2.9	78.6	7.6	10.3	0.6	0.01	2.6	3.5	0.2
After redox in PC	2.8	76.7	6.4	13.3	0.8	0.03	2.3	4.7	0.3

Table 2: Wavelengths of the electronic bands and respective energies and molar extinction coefficients (ε) for pristine poly[1] and WO_3@poly[1] nanocomposites.

Film	Supporting Electrolyte	λ / nm (eV)	ε x 10^{-3} / mol^{-1} dm^3 cm^{-1}
poly[1]	$LiClO_4/CH_3CN$	327 (3.79)	7.24
		402 (3.09)	3.89
		513 (2.42)	**17.27**
		842 (1.47)	6.96
	$LiClO_4$/PC	327 (3.79)	7.21
		398 (3.12)	4.26
		509 (2.44)	**11.35**
		850 (1.46)	6.77
WO_3@poly[1]_s	$LiClO_4/CH_3CN$	325 (3.82)	6.62
		396 (3.13)	3.98
		509 (2.44)	**15.03**
		826 (1.50)	6.40
	$LiClO_4$/PC	325 (3.82)	7.25
		396 (3.13)	4.51
		510 (2.43)	**9.94**
		852 (1.46)	6.53
WO_3@poly[1]_r	$LiClO_4/CH_3CN$	326 (3.81)	6.99
		399 (3.11)	3.85
		511 (2.43)	**15.72**
		840 (1.48)	6.66
	$LiClO_4$/PC	326 (3.81)	7.10
		398 (3.12)	4.11
		510 (2.43)	**9.78**
		848 (1.46)	6.60

Table 3: Optical contrast (ΔT %), change of the optical density (ΔOD), charge requirement (Q_d), and colouration efficiency (η) for pristine poly[1] and WO_3@poly[1] nanocomposite films in $LiClO_4/CH_3CN$ and $LiClO_4$/PC supporting electrolytes, at λ = 750 nm.

Film	Supporting Electrolyte	ΔT%	ΔOD	Q_d / mC cm^{-2}	η / cm^2 C^{-1}
poly[1]	$LiClO_4/CH_3CN$	18.7	0.40	4.50	90.0
	$LiClO_4$/PC	45.5	0.39	4.64	85.0
WO_3@poly[1]_s	$LiClO_4/CH_3CN$	30.8	0.32	2.74	115.2
	$LiClO_4$/PC	39.4	0.33	3.87	85.9
WO_3@poly[1]_r	$LiClO_4/CH_3CN$	31.5	0.30	2.88	103.6
	$LiClO_4$/PC	44.6	0.35	4.33	81.6